



Application of the Godunov-Type Corrective Smoothed Particle Method to Impulsive Load Studies

M. Zhang^{1†} and J. M. Zhang²

¹ Key Laboratory of Microgravity (National Microgravity Laboratory), Institute of Mechanics, Chinese Academy of Sciences, Beijing 100190, P.R. China

² School of Architectural Engineering, Kunming University of Science and Technology, Kunming 650500, P.R. China

†Corresponding Author Email: m_zhang_imcas@163.com

(Received March 18, 2022; accepted August 1, 2022)

ABSTRACT

The smoothed particle hydrodynamics (SPH) method is based on the kernel particle approximation, which is sensitive to the uniformity of the SPH particle distribution in the computational domain; that is, all SPH particles must be distributed evenly in the computational domain. These factors significantly influence the practical application of the SPH method. Meanwhile, calculating the sum near the boundaries of the computational domain may cause boundary defect problems since there are insufficient particles in the support domain, thus often resulting in relatively high errors in numerical simulation results near boundaries. To address these problems, the kernel particle approximation discrete process was corrected based on the traditional SPH method, and the corrected SPH method, the Godunov-type corrective smoothed particle method (CSPM), was formulated by introducing Riemann decomposition. In this study, the traditional SPH method and Godunov-type CSPM method were applied in a comparative study of discontinuous function problems, 1D shock tubes and 1D detonation waves. According to the analysis results, the Godunov-type CSPM method can not only effectively improve the calculation accuracy and compatibility of the traditional SPH method in discontinuous shock wave problems but also increase the accuracy of the traditional SPH method in capturing strong discontinuities.

Keywords: Meshfree method; SPH method; Godunov-type corrective smoothed particle method (GSPM); 1D shock tube; 1D detonation wave.

NOMENCLATURE

A, B, R_1, R_2, ω	fitting coefficients	Δt	time step length
A_{ij}	intersection point	v_{ij}^{*R}	normal velocity at the intersection
c_i	local sound velocity	v_i	SPH particle velocity
e_i	internal energy	V	relative specific volume
$f(x_i)$	field function	W_{ij}	smoothed kernel function
h_i	smooth length	x	Cartesian coordinates
m_i	SPH particle mass	x_i	position of SPH particle
m_{ij}^*	mass at the intersection	x_{ij}^*	position of the intersection
N	SPH particle number	Δx	distance between two adjacent particles
p_i	pressure	γ	ratio of specific heats
p_{ij}^{*R}	pressure at the intersection	ρ_i	SPH particle density
p_{ij}^{*RR}	normal pressure at the intersection	ρ_{ij}^*	density at the intersection
r_{ij}	distance between particles i and j	Ω	support domain

1. INTRODUCTION

Recently, many numerical calculation methods have been developed with the rapid development of computer technology. At present, numerical simulation methods can be divided into mesh-based methods and meshfree methods according to different discretization and solution forms (Sun 2018). Mesh-based methods are easily influenced by mesh distortion when solving large-deformation fluid–structure interaction problems. Meshfree methods are not restricted by the amount of boundary deformation when simulating large-deformation problems due to the advantages of natural Lagrangian characteristics and increasingly perfect particle approximation theory (Liu and Li 2016). Hence, meshfree methods have been extensively applied in high-speed impact problems (Sun 2018). Typical meshfree methods include the discrete element method (DEM) (Chen *et al.* 2020), smoothed particle hydrodynamics (SPH) method (Zheng *et al.* 2020; Gu *et al.* 2016; Ma *et al.* 2012), moving particle semi-implicit (MPS) method (Tian and Wan 2019), etc. The MPS method and SPH method are basically equivalent in solving high-speed impact problems (Hashimoto *et al.* 2022; Abdelrazek *et al.* 2014; Bakti *et al.* 2016). However, since the MPS method is based on the complete incompressible hypothesis (Chen and Wan 2019; Chen *et al.* 2018), it is difficult to apply to problems with obvious compressibility effects, such as the bubble pulsation process of underwater explosions. DEM (Xu *et al.* 2003) is mainly applied to process large-deformation problems of discrete particles (the flow of particles such as grits, ice blocks, etc.) (Sun *et al.* 2013; Robb *et al.* 2016; Kloss *et al.* 2012), and it is inapplicable to study high-speed impact problems. Comparatively, the SPH theory and method have obvious advantages in processing large deformations of fluids and compressibility problems. This method easily performs parallel computation, has strong engineering applicability and is more suitable for solving large-scale high-speed impact problems.

The smoothed particle hydrodynamics (SPH) method proposed by Lucy (1977), Gingold and Monaghan (1977), and Monaghan (1982) is a numerical method in the form of a pure Lagrangian mesh-free method. The core idea of the SPH method lies in interpolation theory. First, the kernel function estimation approximation is performed through an integral kernel called the “smoothed kernel function”. Second, the fluid dynamics control equation set is transformed into the SPH control equation set for numerical calculation. In the whole flow field, fluid media are dispersed into a series of “particles” that carry all physical properties, such as mass, density, velocity, internal energy and pressure intensity. Since these particles can move randomly according to fluid motion laws, the SPH method is theoretically applicable to any deformation problem (Liu and Liu 2003).

Since the traditional SPH method is only applicable to fluid dynamics studies for very short periods (Zhang 1996), it is still in the exploration stage in

terms of boundary processing technology, numerical pressure stability, particle searching efficiency and discontinuous surface (region) processing. For example, restricted by the continuity principle of kernel approximation, particles in the solving domain must be distributed evenly, which is very disadvantageous for applications of the SPH method. There are boundary problems caused by the truncation integral in the kernel approximation. Moreover, there is no particle outside of the boundaries during particle approximation. For the above reasons, there are boundary defects caused by insufficient particles when calculating the sum of particles near boundaries.

Many different solutions have been proposed to effectively process discontinuities and strong discontinuities. In 1999, Chen and Beraun (2000), Liu *et al.* (2002), and Wang *et al.* (2002) proposed a new SPH algorithm from the Taylor series expansion, which was called the corrective smoothed particle method (CSPM). It effectively solves the boundary kernel function interpolation problem, thus improving the calculation accuracy, compatibility and tensile instability of the traditional SPH method. However, the CSPM method requires the equation set to be smooth and continuous in the solving domain, which restricts applications of the CSPM method in the discontinuity problem. Additionally, to solve the low calculation accuracy of artificial viscosity in studies of the traditional SPH method, many scholars have proposed some improvements or alternative methods (Morris and Monaghan 1997; Parshikov and Medin 2002; Monaghan 1997; Inutsuk 1994; Gao *et al.* 2007). Parshikov and Medin (2002) introduced the idea of Godunov discontinuity decomposition into the traditional SPH method and increased the ability of the traditional SPH method to effectively capture discontinuities. However, the algorithm has some limitations. Gao *et al.* (2007) proposed a new SPH method that combined the Godunov discontinuity decomposition idea and the discrete form of the CSPM method (introducing the Riemann solution into the discrete control equation set of the CSPM method)—the Godunov-type corrective smoothed particle method (GSPM). The GSPM solves the difficulties of the CSPM in solving discontinuous fluid dynamics problems and has a higher discontinuity capture accuracy than the traditional SPH method.

In this study, the abovementioned 3 types of SPH methods were summarized. The basic formulas of various methods were deduced thoroughly. Moreover, a comparative study on the discontinuity function, 1D discontinuous shock tube and 1D trinitrotoluene (TNT) explosive denotation was carried out by using the traditional SPH method and GSPM. According to the calculation results, the GSPM increases the strong discontinuity capture accuracy of the traditional SPH method and significantly and effectively relieves the numerical fluctuation of the pressure and density of explosive

products within the computational domain after TNT explosion.

2. BASIC FORMULA OF TRADITIONAL SPH METHOD

The SPH method is used to solve the partial differential equation set based on variable fields such as density, velocity, momentum and energy in fluid dynamics problems. It disperses problem domains defined in the partial differential equation set and calculates functions of variable fields on any point as well as the approximate value of derivatives. Next, it applies the approximation function to the partial differential equation set to obtain a series of discrete ordinary differential equation sets that are only related to time. Finally, it solves the ordinary differential equation set to solve problems.

In the SPH method, the whole system is expressed by independent mass and limited particles occupying independent spaces. Functions and their derivatives must be converted into the discrete form of the superposition sum of all particles in the support domain. Then, the particle approximations of functions and their derivatives at particle i are expressed as:

$$\begin{aligned} \langle f(x_i) \rangle &= \sum_{j=1}^N \frac{m_j}{\rho_j} f(x_j) \cdot W(x_i - x_j, h) \\ &= \sum_{j=1}^N \frac{m_j}{\rho_j} f(x_j) W_{ij} \end{aligned} \quad (1)$$

$$\begin{aligned} \langle \nabla \cdot f(x_i) \rangle &= - \sum_{j=1}^N \frac{m_j}{\rho_j} f(x_j) \cdot \nabla W(x - x_j, h) \\ &= - \sum_{j=1}^N \frac{m_j}{\rho_j} f(x_j) \cdot \nabla_j W_{ij} = \sum_{j=1}^N \frac{m_j}{\rho_j} f(x_j) \cdot \nabla_i W_{ij} \end{aligned} \quad (2)$$

$$\nabla_j W_{ij} = - \nabla_i W_{ij} = - \frac{x_i - x_j}{r_{ij}} \frac{\partial W_{ij}}{\partial r_{ij}} = - \frac{x_{ij}}{r_{ij}} \frac{\partial W_{ij}}{\partial r_{ij}} \quad (3)$$

where $W_{ij} = W(\mathbf{x}_i - \mathbf{x}_j, h) = W(|\mathbf{x}_i - \mathbf{x}_j|, h)$ is called the smoothed kernel function. h is the smooth length which is used to define the sphere of influence of W_{ij} . m_j and ρ_j are the mass and density of particle j ($j = 1, 2, \dots, N$), respectively. N refers to the total number of particles in the support domain of particle i . $r_{ij} = |\mathbf{x}_i - \mathbf{x}_j|$ is the distance between particles i and j .

3. BASIC FORMULA OF CSPM

The corrected smoothed particle method (CSPM) was proposed by [Chen and Beraun \(2000\)](#), [Liu et al. \(2003a\)](#), and [Wang et al. \(2002\)](#) in 1999. The basic idea of CSPM is based on Taylor series expansion. It implements regularization processing to kernel approximation and particle approximation in the traditional SPH method. In other words, kernel estimation in the traditional SPH method is replaced by corrected kernel estimation gained from Taylor series expansion, and then the specific control equation set is dispersed.

First, the function $f(x)$ implements Taylor expansion on one point or one particle in the computational domain. Second, both sides of the function are multiplied by the smooth function $[W_i(x)]$ on the corresponding particle support domain (Ω) at the same time. Third, an integral is carried out on Ω , thus obtaining the kernel particle approximation of $f(x)$ on Ω . Finally, the particle approximation formula of $f(x)$ on Ω is obtained. Similarly, both sides of the Taylor series expansion formula are multiplied by the first-order derivative or high-order derivative of $W_i(x)$ on the corresponding particle support domain (Ω) at the same time. Subsequently, an integral is carried out on Ω , thus obtaining the kernel particle approximation of the first-order derivative or high-order derivative of $f(x)$ on Ω . Finally, the particle approximation formula of the first-order derivative or high-order derivative of $f(x)$ on Ω can be obtained.

Given a 1D computational domain, suppose that $f(x)$ is fully smooth in the interval Ω of particle i . Then, it gains the following formula through a Taylor series expansion of $f(x)$ on point x_i at particle i in the computational domain:

$$\begin{aligned} f(x) &= f(x_i) + (x - x_i) f_x(x_i) + \\ &\frac{(x - x_i)^2}{2!} f_{xx}(x_i) + \dots \end{aligned} \quad (4)$$

where $f_i = f(x_i)$, $f_{xi} = f_x(x_i) = (df/dx)_i$, $f_{xxi} = f_{xx}(x_i) = (d^2f/dx^2)_i$.

Both sides of Eq. (4) are multiplied by $W_i(x)$ which is defined on the local support domain (Ω) of particle i . Next, the integral of Ω is obtained:

$$\begin{aligned} \int_{\Omega} f(x) W_i(x) dx &= f(x_i) \int_{\Omega} W_i(x) dx + f_x(x_i) \int_{\Omega} (x - x_i) W_i(x) dx + \\ &\frac{f_{xx}(x_i)}{2!} \int_{\Omega} (x - x_i)^2 W_i(x) dx + \dots \end{aligned} \quad (5)$$

If the first-order and higher-order derivatives of $f(x)$ in Eq. (5) are ignored, the corrected formula of the kernel particle approximation of $f(x)$ on point x_i in the computational domain is:

$$f(x_i) \cong \frac{\int_{\Omega} f(x) W_i(x) dx}{\int_{\Omega} W_i(x) dx} \quad (6)$$

Similarly, both sides of Eq. (4) are multiplied by the first-order derivative of $W_i(x)$ on the local support domain (Ω) of the corresponding particle. In other words, $W_{i,x}(x) = \partial W_i(x)/\partial x$ is used to replace the first-order derivative of $W_i(x)$, while the second-order and higher-order derivatives of $f(x)$ in Eq. (5) are ignored. In this way, the corrected formula of the first-order kernel particle approximation of $f(x)$ on point x_i at particle i in the computational domain is:

$$f_x(x_i) \cong \frac{\int_{\Omega} [f(x) - f(x_i)] W_{i,x}(x) dx}{\int_{\Omega} (x - x_i) W_{i,x}(x) dx} \quad (7)$$

The numerators in Eq. (6) and Eq. (7) are indeed the kernel particle approximation formula of the

function and the first-order derivatives in the traditional SPH method, while denominators (regularization factor) are descriptions of regularized properties of $W_i(x)$, which is defined on Ω of particle i . Hence, the corrected kernel particle approximation gained by CSPM is gained through regularization based on the kernel particle approximation formula, which is gained by the traditional SPH method.

Moreover, it must be noted that when the boundaries of the support domain and computational domain of particle i are independent from each other, the integral of the corresponding $W_i(x)$ on Ω is 1. When the boundaries of the support domain and computational domain of particle i intersect, the integral of the corresponding $W_i(x)$ on Ω is not 1. Obviously, for any particle i in the computational domain, the truncation errors of the field function $f(x_i)$ and its first-order derivative with respect to x [$f_x(x_i)$] are $(x - x_i)^2$ order. For any particle i on boundaries or near boundaries of the computational domain, the truncation errors of $f(x_i)$ and $f_x(x_i)$ are $(x - x_i)$ orders. In other words, particles in the computational domain are first-order continuous, and particles on boundaries or near boundaries of the computational domain are zero-order continuous. Moreover, the premise of such continuity is to ensure that all SPH particles are distributed uniformly in the computational domain.

Therefore, the description of the regularization properties of $W_i(x)$, which are defined on Ω of particle i , is ignored, or it hypothesizes that all integrals of $W_i(x)$ on Ω in regard to any particle in the computational domain meeting the regularization conditions are the essential causes of boundary defects in the traditional SPH method.

The continuous integral expressions in Eq. (6) and Eq. (7) are rewritten as the sum expressions at the discrete point, thus obtaining the particle approximation on particle i .

$$f(x_i) \cong \frac{\sum_{j=1}^N \left(\frac{m_j}{\rho_j}\right) f(x_j) W_{ij}}{\sum_{j=1}^N \left(\frac{m_j}{\rho_j}\right) W_{ij}} \quad (8)$$

$$f_x(x_i) \cong \frac{\sum_{j=1}^N \left(\frac{m_j}{\rho_j}\right) [f(x_j) - f(x_i)] \nabla_j W_{ij}}{\sum_{j=1}^N \left(\frac{m_j}{\rho_j}\right) (x_j - x_i) \nabla_j W_{ij}} = \frac{\sum_{j=1}^N \left(\frac{m_j}{\rho_j}\right) [f(x_j) - f(x_i)] W_{ij,x}}{\sum_{j=1}^N \left(\frac{m_j}{\rho_j}\right) (x_j - x_i) W_{ij,x}} \quad (9)$$

where $W_{ij,x} = \partial W_{ij} / \partial x_j$.

Through the above introduction to the CSPM based on the correction of the traditional SPH method, the CSPM discrete form of the 1D fluid dynamics control equation set can be gained by using the CSPM:

$$\rho_i = \frac{\sum_{j=1}^N m_j W_{ij}}{\sum_{j=1}^N \left(\frac{m_j}{\rho_j}\right) W_{ij}} \quad (10)$$

$$\frac{d\rho_i}{dt} = -\rho_i \frac{\sum_{j=1}^N \left(\frac{m_j}{\rho_j}\right) (v_j - v_i) W_{ij,x}}{\sum_{j=1}^N \left(\frac{m_j}{\rho_j}\right) (x_j - x_i) W_{ij,x}} \quad (11)$$

$$\frac{dv_i}{dt} = -\frac{1}{\rho_i} \frac{\sum_{j=1}^N \left(\frac{m_j}{\rho_j}\right) (p_j - p_i) W_{ij,x}}{\sum_{j=1}^N \left(\frac{m_j}{\rho_j}\right) (x_j - x_i) W_{ij,x}} \quad (12)$$

$$\frac{de_i}{dt} = -\frac{p_i}{\rho_i} \frac{\sum_{j=1}^N \left(\frac{m_j}{\rho_j}\right) (v_j - v_i) W_{ij,x}}{\sum_{j=1}^N \left(\frac{m_j}{\rho_j}\right) (x_j - x_i) W_{ij,x}} \quad (13)$$

Based on the above equations, differences between CSPM and the traditional SPH method are manifested by different structures of the integral expressions of kernel particle approximation. Moreover, kernel particle approximation and particle approximation in CSPM are connected with those in the traditional SPH method through numerators. The denominators describe the regularization properties of $W_i(x)$, which are defined on Ω of particle i .

4. BASIC FORMULA OF THE GODUNOV-TYPE CSPM

Although the CSPM method achieves more accurate and reliable results in a series of practical applications compared to the traditional SPH method, the basic approximation idea of the CSPM is based on the Taylor series expansion of the kernel function. This requires the control equation set to meet full smoothness and continuity on the whole computational domain. Hence, the applications of CSPM to discontinuity problems (e.g., shock wave) are restricted significantly. For effective applications of the CSPM method to the discontinuity problem, Gao *et al.* (2007) proposed a new SPH method based on the combination of the Godunov discontinuity decomposition idea and discrete forms of the CSPM method (introducing the Riemann solution into the discrete control equation set of CSPM) in 2007. This is known as the Godunov-type CSPM (GSPM).

First, it hypothesizes that all physical properties of SPH particles in the support domain are in constant distribution and that the support domains of particles are spherical. The support domains of each particle are tangent ($j = 1$), intersecting ($j = 3$) or separated ($j = 2$) pairwise. Moreover, the connection line (ij) between particles i and j is perpendicular to the interface of the support domains of each particle. The intersection point between line ij and the interface is expressed by A_{ij} (when support domains of two particles intersect or separate, the

position of intersection is determined by the radius proportion of the support domain of corresponding particles). The velocity (v_{ij}^{*R}) and pressure (p_{ij}^{*R}) at A_{ij} can be calculated by the results expressed in the sound velocity approximation for the Riemann solution, which was proposed by Godunov in 2002. In addition, particles i and j exchange momentum and energy on the interface (Fig. 1 and Fig. 2). It can be seen from the above hypothesis that particles i and j form a Riemann problem. The initial discontinuity surface of this Riemann problem is:

$$(e, \rho, p) = \begin{cases} (e, \rho, p)_j^* & (x \in \text{particle } j) \\ (e, \rho, p)_i^* & (x \in \text{particle } i) \end{cases} \quad (14)$$

This initial discontinuity surface moves toward two sides at the local sound velocities of c_j and c_i . Moreover, the velocity and pressure intensity of particles are equal within the region scanned by shock waves. Next, the normal velocity and pressure intensity on the discontinuous interface can be calculated according to the mass and momentum conservation equation. The expressions are:

$$v_{ij}^{*R} = \frac{\rho_j c_j v_j^R + \rho_i c_i v_i^R - (p_j - p_i)}{\rho_j c_j + \rho_i c_i} \quad (15)$$

$$p_{ij}^{*R} = \frac{\rho_j c_j p_i + \rho_i c_i p_j - \rho_j c_j \rho_i c_i (v_j^R - v_i^R)}{\rho_j c_j + \rho_i c_i} \quad (16)$$

$$c_i = \sqrt{\frac{\gamma P_i}{\rho_i}} \quad (17)$$

where $\gamma = 1.4$.

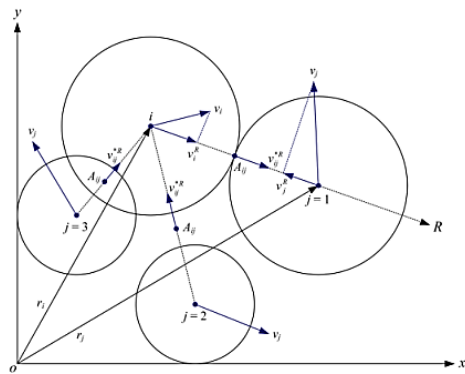


Fig. 1. Interaction diagram of SPH particles in the GSPM.

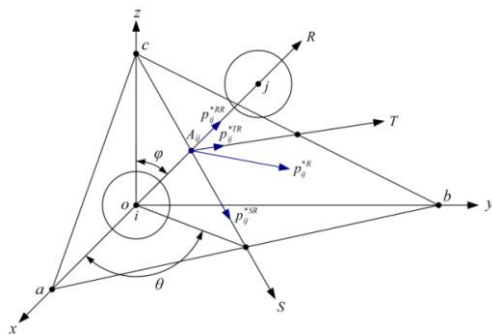


Fig. 2. RST coordinate system and pressure distributions on interface abc.

Parshikov and Medin (2002) suggested replacing velocity (v_j^R) and pressure (p_j) in Eq. (15) and Eq. (16) by $2 v_{ij}^{*R} - v_i^R$ and $2 p_{ij}^{*R} - p_i$ (Riemann solution) in the traditional SPH method, respectively. Nevertheless, it can be found from the calculated results that through the above method, the Riemann solution can be introduced in the discrete expression of CSPM to calculate the 1D shock wave problem. The position of the captured shock wave array deviates from the known accurate solution to some extent. It was discovered from a numerical experiment that such deviation is mainly caused by asymmetric momentum and energy exchange between two adjacent SPH particles in the CSPM discrete control equation set. However, the control equation set deduced from the CSPM makes it difficult to obtain a group of discrete expressions with symmetric momentum and energy exchange between two adjacent SPH particles.

For this reason, Gao *et al.* (2007) designed another method to introduce the Riemann solution: the physical properties of SPH particle j in the discrete expression, which is gained through CSPM, are directly replaced by the Riemann solution at the discontinuity surface, considering the displacement of the discontinuity surface.

Based on the volume ratio of the support domains of two contacting particles and the displacement of the contact discontinuous surface of two connecting particle support domains, the position of the contacting discontinuity surfaces (x_{ij}^*) is obtained, and its expression is:

$$x_{ij}^* - x_i = (x_j - x_i) \left(\frac{\frac{m_i}{\rho_i}}{\frac{m_i}{\rho_i} + \frac{m_j}{\rho_j}} \right) + v_{ij}^{*R} \Delta t \quad (18)$$

Based on the volume average of two contacting particle support domains, the density (ρ_{ij}^*) at the contacting discontinuous surfaces can be expressed as:

$$\rho_{ij}^* = \frac{m_i + m_j}{v_i + v_j} \quad (19)$$

Through the particle mass arithmetic mean of two contacting particle support domains, the mass (m_{ij}^*) at the contacting discontinuous surfaces is expressed as:

$$m_{ij}^* = \frac{1}{2}(m_i + m_j) \quad (20)$$

The normal velocity and pressure intensity at the contacting discontinuous surfaces are gained through Eq. (15) and Eq. (16), respectively.

The physical properties of all SPH particles (j) in discrete expressions (11) - (13) gained through CSPM are replaced by physical properties at contacting discontinuous surfaces, which are obtained by introducing the Riemann solution. In this way, a group of new Godunov-type CSPM discrete control equation sets can be obtained, that is, GSPM discrete expressions:

$$\frac{d\rho_i}{dt} = -\rho_i \frac{\sum_{j=1}^N \left(\frac{m_{ij}^*}{\rho_{ij}^*}\right) (v_{ij}^{*R} - v_i) W_{ij,x}}{\sum_{j=1}^N \left(\frac{m_{ij}^*}{\rho_{ij}^*}\right) (x_{ij}^* - x_i) W_{ij,x}} \quad (21)$$

$$\frac{dv_i}{dt} = -\frac{1}{\rho_i} \frac{\sum_{j=1}^N \left(\frac{m_{ij}^*}{\rho_{ij}^*}\right) (p_{ij}^{*RR} - p_i) W_{ij,x}}{\sum_{j=1}^N \left(\frac{m_{ij}^*}{\rho_{ij}^*}\right) (x_{ij}^* - x_i) W_{ij,x}} \quad (22)$$

$$\frac{de_i}{dt} = -\frac{p_i}{\rho_i} \frac{\sum_{j=1}^N \left(\frac{m_{ij}^*}{\rho_{ij}^*}\right) (v_{ij}^{*R} - v_i) W_{ij,x}}{\sum_{j=1}^N \left(\frac{m_{ij}^*}{\rho_{ij}^*}\right) (x_{ij}^* - x_i) W_{ij,x}} \quad (23)$$

5. CASE VERIFICATION AND COMPARISON OF RESULTS

5.1 Discontinuous Function Problems

A numerical verification of the GSPM was carried out by using the following discontinuous function.

$$f(x) = \begin{cases} x^2 & -1 \leq x \leq 0.5 \\ -0.5 - x^2 & 0.5 < x \leq 1 \end{cases} \quad (24)$$

The first-order derivative of the discontinuous function with respect to x is:

$$\frac{df(x)}{dx} = \begin{cases} 2x & -1 \leq x \leq 0.5 \\ -2x & 0.5 < x \leq 1 \end{cases} \quad (25)$$

Discretization was implemented in Eq. (24) and Eq. (25) by using the traditional SPH method and GSPM, respectively. In addition, the SPH method and GSPM both apply the smoothed kernel function in cubic spline form. SPH particles are in uniform distribution on the problem domain $[-1, 1]$. The volume (Δx_i) of each particle is 0.05. In other words, there are a total of 40 SPH particles in the problem domain. To better show the advantages and disadvantages of various methods in boundary processing, the boundaries of the discontinuous function and its first-order derivative with respect to x were not processed in this study.

The calculated results of the discontinuous function and the first-order derivative with respect to x after discretization by the two types of SPH methods are shown in Fig. 3 and Fig. 4. It can be seen that:

The calculated results of the traditional SPH method at the discontinuous point of the discontinuous function and its first-order derivative with respect to x deviate significantly from accurate values. Moreover, there are obvious boundary defects at the boundaries.

The GSPM not only obtains calculated results of the discontinuous point of the discontinuous function and its first-order derivative with respect to x in high accordance with accurate values but also solves boundary defects well. This indicates that the GSPM introduced in Riemann solutions into the traditional SPH method can not only solve

discontinuous problems in the computational domain but also solve boundary defects caused by insufficient SPH particles near boundaries. Moreover, the calculated results have very high accuracy.

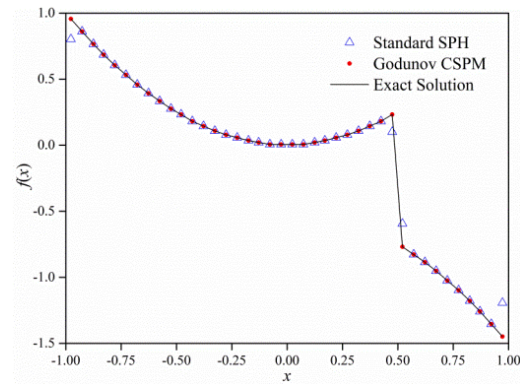


Fig. 3. Discrete approximation results of the discontinuous function in Eq. (24).

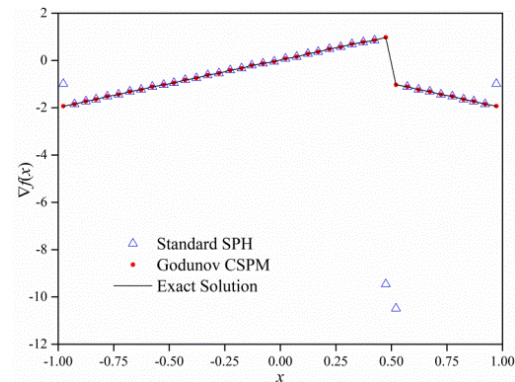


Fig. 4. Discrete approximation results of the first-order derivative of the discontinuous function with respect to x in Eq. (25).

5.2 Discontinuous Shock Tube Problems

In the above case, the calculated results of GSPM in processing discontinuous problems in the computational domain have very high accuracy. In this case, two types of SPH methods were applied to process 1D discontinuous shock tube problems. Now, there are exact solutions to the 1D discontinuous shock tube problems. Hence, this case is used to test the superiority of the GSPM in solving shock load problems.

The 1D discontinuous shock tube refers to a long straight tube filled with gas. The gas in the tube is divided into two parts with different pressures and densities by a diaphragm. In each part, gas is in the equilibrium state in the beginning in terms of pressure, density and temperature (Fig. 5). When the diaphragm is removed suddenly, a shock wave, expansion fans and discontinuous contact region are produced in the shock tube. Specifically, the shock wave enters the region with a lower gas density, while the expansion fans move to the region with a higher gas density. Meanwhile, a discontinuous contact region will be formed near the center of the shock tube. Subsequently, this region follows the

shock wave continuously to move to the low-density region (Fig. 6).

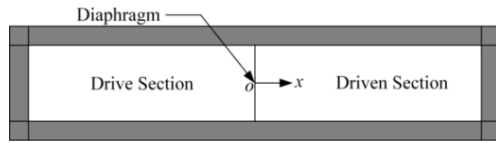


Fig. 5. Shock tube diagram before breakage of the diaphragm.

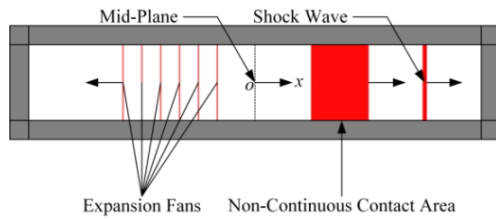


Fig. 6. Various physical phenomena are produced in the shock tube after breakage of the diaphragm.

The specific model used in this case is $x \leq 0$ m, $\rho = 1$ kg/m³, $v = 0$ m/s, $e = 2.5$ J/kg, $p = 1$ Pa, $\Delta x = 0.001875$ m; $x > 0$ m, $\rho = 0.25$ kg/m³, $v = 0$ m/s, $e = 1.795$ J/kg, $p = 0.1795$ Pa, and $\Delta x = 0.0075$ m. Specifically, v , p , ρ and e are velocity, pressure, density and internal energy, respectively. Δx refers to the distance between two adjacent SPH particles.

In this case model, 320 SPH particles are distributed uniformly along $[-0.6$ m, 0.0 m], and 80 SPH particles are distributed uniformly along $[0.0$ m, 0.6 m]. In other words, there are uneven distribution problems of SPH particles along the shock tube (positive direction of the x axis), and the mass of SPH particles is the same: $m_i = 0.001875$ kg. The ideal gas state equation is used as the state equation of gas in the shock tube: $p = (\gamma - 1)\rho e$, where $\gamma = 1.4$. Two types of SPH methods both use the smoothed kernel function in the cubic spline form and the smooth length (h) is kept constant: the average distance between two adjacent SPH particles. Adjacent particles searching uses the full pairwise searching method, and the time integral calculation uses the leapfrog format calculation method [Eq. (26)]. Curve distribution patterns of velocity, pressure intensity, density and internal energy of SPH particles in shock tube along the shock tube (positive direction of x axis) at $t = 0.2$ s are shown in Fig. 7, Fig. 8, Fig. 9 and Fig. 10, respectively.

$$\begin{cases} t = t + \Delta t \\ \rho_i \left(t + \frac{\Delta t}{2} \right) = \rho_i \left(t - \frac{\Delta t}{2} \right) + D\rho_i(t) \Delta t \\ e_i \left(t + \frac{\Delta t}{2} \right) = e_i \left(t - \frac{\Delta t}{2} \right) + De_i(t) \Delta t \\ v_i \left(t + \frac{\Delta t}{2} \right) = v_i \left(t - \frac{\Delta t}{2} \right) + Dv_i(t) \Delta t \\ x_i \left(t + \frac{\Delta t}{2} \right) = x_i(t) + v_i \left(t + \frac{\Delta t}{2} \right) \Delta t \end{cases} \quad (26)$$

where $D = \partial/\partial t$.

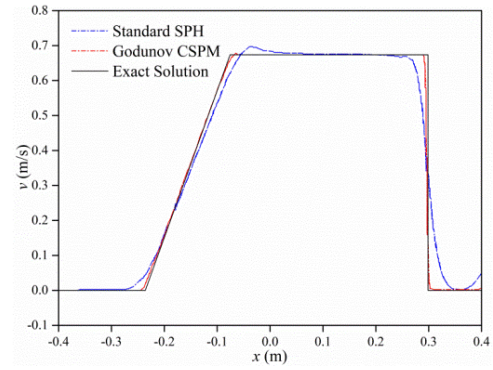


Fig. 7. Velocity distribution for the discontinuous shock tube problem obtained using two versions of the SPH formulation.

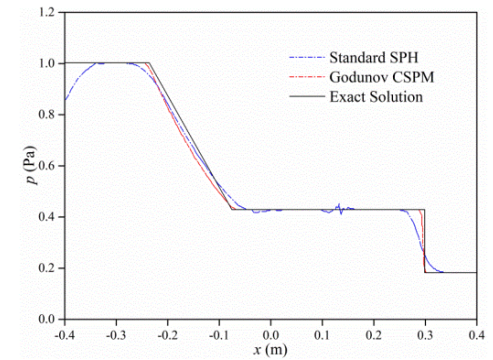


Fig. 8. Pressure intensity distribution for the discontinuous shock tube problem obtained using two versions of the SPH formulation.

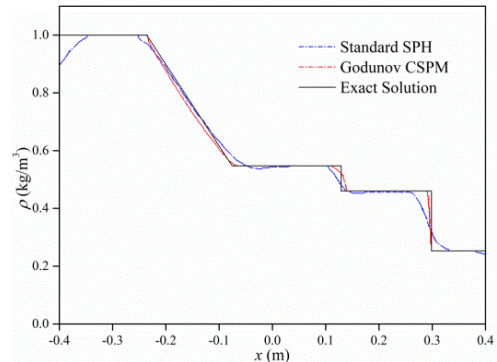


Fig. 9. Density distribution for the discontinuous shock tube problem obtained using two versions of the SPH formulation.

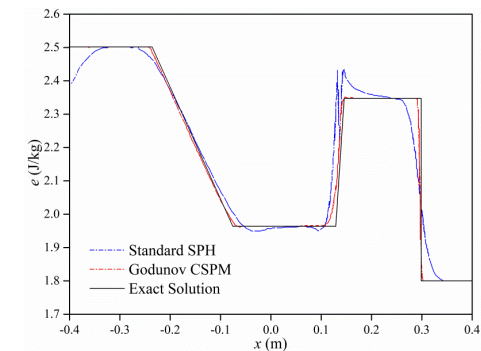


Fig. 10. Internal energy distribution for the discontinuous shock tube problem obtained using two versions of the SPH formulation.

It can be seen from the above curve distributions that the shock wave surface (shock wave array) is near $x = 0.3$ m and the expansion fans are between $x = -0.3$ m and $x = 0$. The discontinuous distribution region of SPH particles is between $x = 0.1$ m and $x = 0.2$ m.

For the traditional SPH method, if SPH particles in the computational domain are not uniformly distributed in the beginning and the smoothed kernel function or its first-order derivative with respect to x is not sufficiently smooth, the calculated results of the corresponding physical properties in the domain may show serious nonphysical fluctuations. The above curve distributions show that in the computational domain (discontinuous contact region) with uneven SPH particle distributions, the calculated results of the traditional SPH method in the domain present obvious nonphysical fluctuations.

It can also be seen from the above curve distributions that the calculated results of the GSPM in the computational domain (discontinuous contact region) within uneven SPH particle distributions and at the strong discontinuity point are more stable. GSPM solves the numerical fluctuation of the traditional SPH method in the computational domain with uneven SPH particle distributions well. Moreover, the calculated results of the GSPM at the strong discontinuity point are closer to an accurate solution.

Based on a comparison of the above two types of SPH methods, the GSPM can effectively solve the numerical simulation difficulties of the traditional SPH method in computational fluid dynamics fields, such as in the computational domain (discontinuous contact region) within uneven SPH particle distributions and at strong discontinuity points. Moreover, the calculated results are closer to the accurate solution. Therefore, the GSPM promotes the accuracy of the traditional SPH method in strong discontinuity capture.

5.3 Slatted TNT Detection Problems

The specific model used in this case study is introduced as follows: the 1D slatted TNT explosive is approximately 0.2 m long, and the slatted TNT explosive is detonated from the middle to two ends. Before detonation, SPH particles distribute uniformly along the geometric model of the 1D slatted TNT explosive, and there are 1,000 SPH particles. The initial density of the TNT explosive is $\rho_0 = 1630$ kg/s. In this study, the Jones–Wilkins–Lee (JWL) state equation [Eq. (27)] was used as the state equation of TNT explosive products, while the state equation of air uses the ideal gas state equation. Two types of SPH methods used the smoothed kernel function in the cubic spline form, and the initial smooth length (h_0) was 1.5 times that of the average distance between two adjacent SPH particles. Iterative updating was carried out through Eq. (28), and the full pairing searching method was applied for nearby particle searching. The time integral calculation uses the leapfrog mesh computing method, and the time step length is $\Delta t = 1.0 \times 10^{-9}$ s. At the moment of slatted TNT explosive

denotation, the denotation products diffuse from the middle, and the detonation wave array in the spherically asymmetric distribution is produced. The kinematic velocity was 6930 m/s, and the whole detonation process ended after approximately 14.4 μ s (Fig. 11).

$$p = A \left(1 - \frac{\omega}{R_1 V} \right) e^{-R_1 V} + B \left(1 - \frac{\omega}{R_2 V} \right) e^{-R_2 V} + \frac{\omega e}{V} \quad (27)$$

$$\frac{dh_i^n}{dt} = -\frac{h_i^n}{\rho_i^n} \frac{d\rho_i^n}{dt} = -\frac{h_i^n}{\rho_i^n} \sum_{j=1}^N m_j (v_i^n - v_j^n) \cdot \nabla_i^n W_{ij} \quad (28)$$

where p is the pressure of detonation products of the TNT explosive and V is the relative specific volume of detonation products of the TNT explosive. A , B , R_1 , R_2 and ω are fitting coefficients related to the state of TNT explosives. e refers to the specific thermodynamic energy. h_i^n , ρ_i^n , v_i^n and $\nabla_i^n W_{ij}$ are the smooth length, density, and velocity of SPH particle i in the n th time step as well as the gradient of the smoothed kernel function, respectively.

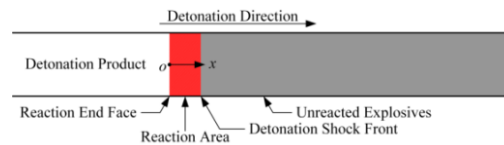


Fig. 11. Detonation process of the 1D slatted TNT explosive detonation model.

Curve distributions of numerical simulation results of pressure and density of each SPH particle along the geometric model (positive direction of x -axis) at $t = 4 \mu$ s and $t = 12 \mu$ s during detonation of the 1D slatted TNT explosive are shown in Fig. 12 and Fig. 13, respectively. In this case, the pressure and density of the products after detonation of the 1D slatted TNT explosive at the Chapman–Jouguet (C–J) point have theoretical approximate analytical solutions of 19.57 GPa and 2173 kg/m³, respectively. The C–J peak of detonation product pressure was calculated to be 21 GPa by Liu *et al.* (2003b) through an experimental method.

For the traditional SPH method, it can be seen from the numerical simulation results that the pressure and density of detonation products from the 1D slatted TNT explosive at the C–J point are very close to the theoretical values or experimental values. In addition, the pressure value of detonation products on the C–J point at $t = 12 \mu$ s is between the experimental value and theoretical value, which is enough to elaborate that in the processing detonation problem of a 1D slatted TNT explosive, the calculated results of the traditional SPH method conform to the practical variation law. The traditional SPH method can accurately predict the shape and size of the detonation wave as well as the pressure peak on the C–J point and pressure distribution during detonation of a 1D slatted TNT explosive. However, after finishing detonation of a one-dimensional slatted TNT explosive, numerical values of pressure and density of detonation products fluctuate slightly within the computational domain.

Compared with the traditional SPH method, the numerical simulation results of the pressure and density of detonation products on the C–J point in the GSPM method are also very close to the experimental values or theoretical values. In addition, the pressure peak of detonation products on the C–J point is closer to the experimental or theoretical results. After finishing the detonation of the 1D slatted TNT explosive, the small fluctuation of numerical pressure and density values of detonation products within the computational domain is relieved effectively (Fig. 12 and Fig. 13). Therefore, the GSPM method is also applicable to solving the shock wave of detonation, and numerical simulation results could achieve higher accuracy.

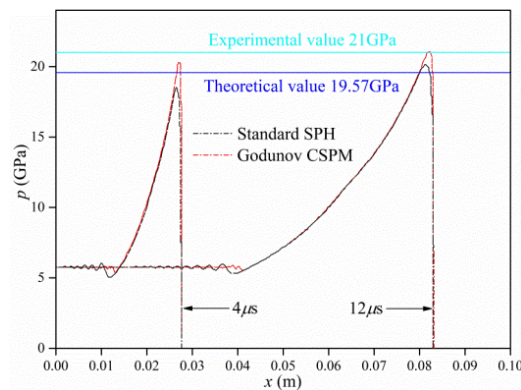


Fig. 12. Pressure intensity distributions at 4 μ s and 12 μ s obtained using two versions of the SPH formulation.

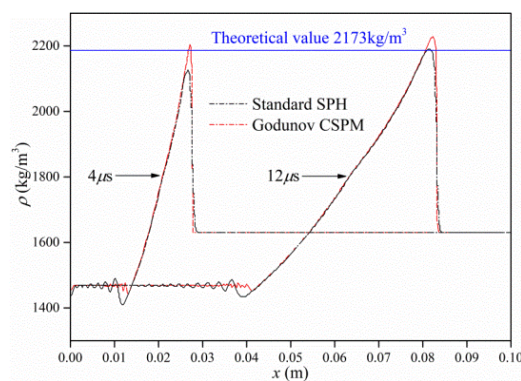


Fig. 13. Density distributions at 4 μ s and 12 μ s obtained using two versions of the SPH formulation.

The variations in total internal energy per unit mass, total kinetic energy per unit mass and initial total energy per unit mass in the GSPM with detonation time are shown in Fig. 14. Obviously, as the detonation continues, the total kinetic energy per unit mass increases gradually, while the total internal energy per unit mass declines. However, the initial total energy per unit mass is kept as an approximate constant, approximately 6.9927 MJ/kg. The relative error of total energy per unit mass has been kept lower than 0.01%, indicating that the GSPM method has very good numerical stability.

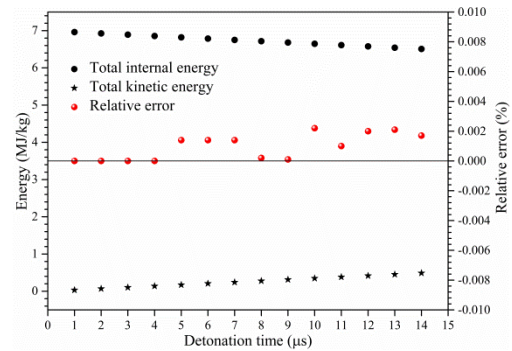


Fig. 14. Time history of energy balance.

Finally, to further discuss the influences of the SPH particle distribution density (total number of SPH particles) on the calculated results of the GSPM, the number of SPH particles was set as 250, 500, 1000, 2000 and 4000 in the numerical simulation in the 0.2 m long 1D slatted TNT explosive detonation model, which detonates from the middle. According to the different distribution densities of SPH particles, the time step length for the calculation of the numerical integral was adjusted accordingly. Finally, the influences of the SPH particle number on the pressure peak, energy peak, density peak and velocity peak of detonation products from the 1D slatted TNT explosive during 1 μ s and 14 μ s were acquired. For convenient observation, a diagram was plotted according to the peak points of several physical properties every 1 μ s from 1 μ s to 14 μ s, which can intuitively reflect the influences of the SPH particle number on the calculated results of the GSPM. The results are shown in Figs. 15, 16, 17 and 18.

It can be seen from numerical simulation results that the pressure peak, velocity peak and density peak of detonation products when finishing detonation approach the experimental value or theoretical value with the increase in the SPH particle number (among them, the density peak agrees best with the theoretical value). This reveals that the distribution density of SPH particles has a direct influence on the accuracy of the numerical simulation results. Theoretically, the detonation model of a 1D slatted TNT explosive can reflect the internal structure of materials more accurately when there are more SPH particles (smaller distance between two adjacent SPH particles). Hence, the fluctuation in the numerical shock wave pressure generated by the detonation of explosives during spreading among SPH particles is smaller, and the calculated results are more accurate. This is verified by the above numerical simulation results. Nevertheless, increasing the number of SPH particles introduces a disadvantage to numerical simulation while increasing the calculation accuracy: it must make one nearby particle search for all SPH particles in the computational domain within each time step. As a result, this method is applicable when there are few SPH particles. With the gradual growth of SPH particles, it takes a longer time for numerical simulation, thus decreasing computational efficiency. Obviously, selecting the density of SPH particles is recommended when using the GSPM

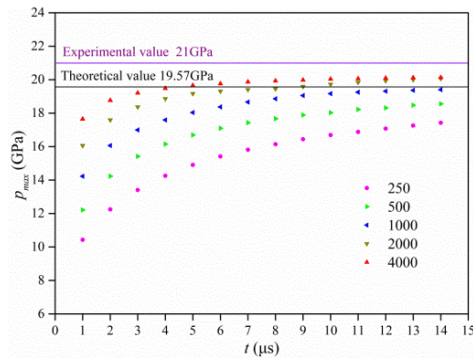


Fig. 15. Influences of the SPH particle number on the pressure peak of products after detonation of a 1D slatted TNT explosive.

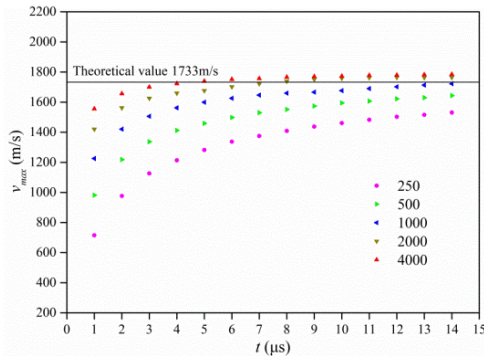


Fig. 16. Influences of the SPH particle number on the velocity peak of products after detonation of a 1D slatted TNT explosive.

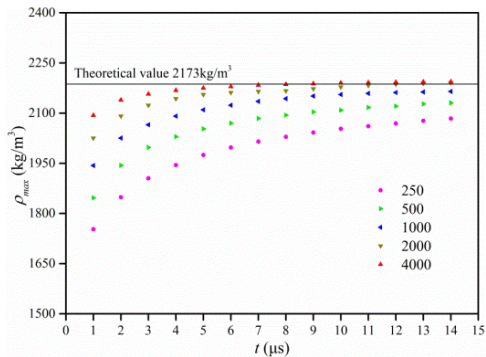


Fig. 17. Influences of the SPH particle number on the density peak of products after detonation of a 1D slatted TNT explosive.

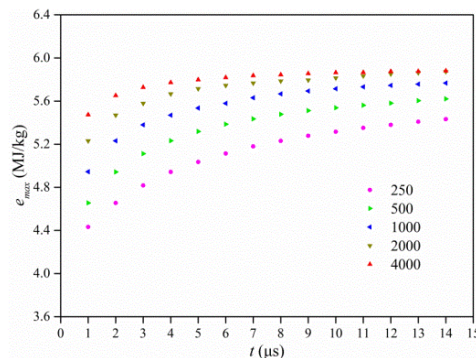


Fig. 18. Influences of the SPH particle number on the energy peak of products after detonation of a 1D slatted TNT explosive.

method to solve shock wave problems. This not only can predict the characteristics of the shock wave and pressure distribution in the detonation process relatively accurately but can also improve the computational efficiency.

6. CONCLUSIONS

This study mainly corrected the kernel particle approximation of the traditional SPH method and thereby obtained the CSPM after normalized correction of the kernel particle approximation and particle approximation. Later, a new SPH method is developed based on a combination of the Godunov discontinuous decomposition idea and the discrete form of CSPM (introducing the Riemann solution into the discrete control equation set of CSPM), which is known as the GSPM. Moreover, the GSPM is applied to solve the discontinuous function problem, 1D shock tube problem and detonation shock wave problem. It can be seen from numerical verification and comparative calculation that the GSPM is significantly superior to the traditional SPH method in terms of calculation accuracy and numerical fluctuation in processing discontinuous problems. Moreover, the GSPM can well solve the numerical simulation difficulties of the traditional SPH method in the computational domain (discontinuous contact area) with uneven SPH particle distributions and at the strong discontinuity point. As a result, the GSPM increases the accuracy of the traditional SPH method in strong discontinuity capture. It provides a new method to study discontinuity phenomena such as shock waves.

ACKNOWLEDGEMENTS

This work was financially supported by the National Natural Science Foundation of China (Grants 11261026, 11532015, and U1738119), which are gratefully acknowledged.

REFERENCES

- Abdelrazek, A. M., I. Kimura and Y. Shimizu (2014). Comparison between SPH and MPS methods for numerical simulations of free surface flow problems. *Journal of Japan Society of Civil Engineers, Ser. B1 (Hydraulic Engineering)* 70(4), I_67-I_72.
- Bakti, F. P., M. H. Kim, K. S. Kim and J. C. Park (2016). Comparative study of standard WC-SPH and MPS solvers for free surface academic problems. *International Journal of Offshore and Polar Engineering* 26(3), 235–243.
- Chen, J. K. and J. E. Beraun (2000). A generalized smoothed particle hydrodynamics method for nonlinear dynamic problems. *Computer Methods in Applied Mechanics and Engineering* 190(1/2), 225–239.
- Chen, X. and D. C. Wan (2019). Numerical

- simulation of liquid sloshing in LNG tank using GPU-accelerated MPS method. *Chinese Journal of Theoretical and Applied Mechanics* 51(3), 714–729.
- Chen, X., Y. L. Zhang and D. C. Wan (2018). Developments of the MPS method and its applications on hydrodynamics problems. *Journal of Harbin Engineering University* 39(6), 955–972.
- Chen, Y. D., F. Lu, H. S. Sun, C. Z. Gong, M. B. Cao, and J. D. Cai (2020). Study on bearing behavior of uplift pile based on discrete element method. *Water Resources and Hydropower Engineering* 51(9), 200–204.
- Gao, W. R., H. F. Qiang and S. Y. Zhang (2007). Godunov-type corrective smoothed particle method (CSPM). *Chinese Journal of Computational Mechanics* 24(5), 638–642.
- Gingold, R. A. and J. J. Monaghan (1977). Smoothed particle hydrodynamics: theory and application to non-spherical stars. *Monthly Notices of the Royal Astronomical Society* 181(3), 375–389.
- Gu, S. L., Y. S. Wu, H. W. Xie and X. W. Yuan (2016). CSPM method-based numerical simulation on outflow from 2-D pipe nozzle. *Water Resources and Hydropower Engineering* 47(9), 39–43.
- Hashimoto, H., N. Grenier, M. Sueyoshi and D. L. Touze (2022). Comparison of MPS and SPH methods for solving forced motion ship flooding problems. *Applied Ocean Research* 118, 103001.
- Inutsuka, S. (1994). Godunov-type SPH. *Memorie Della Societa Astronomica Italiana* 65(4), 1027–1031.
- Kloss, C., C. Goniva, A. Hager, S. Amberger and S. Pirker (2012). Models, algorithms and validation for opensource DEM and CFD-DEM. *Progress in Computational Fluid Dynamics an International Journal* 12(2/3), 140–152.
- Liu, G. R. and M. B. Liu (2003). *Smoothed Particle Hydrodynamics: A Meshfree Particle Method*. Singapore: World Scientific Publishing Co. Pte. Ltd.
- Liu, M. B. and S. M. Li (2016). On the modeling of viscous incompressible flows with smoothed particle hydro-dynamics. *Journal of Hydrodynamics, Ser. B* 28(5), 731–745.
- Liu, M. B., G. R. Liu and K. Y. Lam (2003a). A one-dimensional meshfree particle formulation for simulating shock waves. *Shock Waves* 13(3), 213–220.
- Liu, M. B., G. R. Liu, K. Y. Lam and Z. Zong (2003b). Smoothed particle hydrodynamics for numerical simulation of underwater explosion. *Computational Mechanics* 30(2), 106–118.
- Lucy, L. B. (1977). A numerical approach to the testing of the fission hypothesis. *The Astronomical Journal* 82(12), 1013–1024.
- Ma, L. Q., M. B. Liu, J. Z. Chang, T. X. Su and H. T. Liu (2012). Numerical simulation of droplet impact onto liquid films with smoothed particle hydrodynamics. *Acta Physica Sinica* 61(24), 244701.
- Monaghan, J. J. (1982). Why particle methods work. *SIAM Journal on Scientific & Statistical Computing* 3(4), 422–433.
- Monaghan, J. J. (1997). SPH and Riemann solvers. *Journal of Computational Physics* 136(2), 298–307.
- Morris, J. P. and J. J. Monaghan (1997). A switch to reduce SPH viscosity. *Journal of Computational Physics* 136(1), 41–50.
- Parshikov, A. N. and S. A. Medin (2002). Smoothed particle hydrodynamics using interparticle contact algorithms. *Journal of Computational Physics* 180(1), 358–382.
- Robb, D. M., S. J. Gaskin and J. C. Marongiu (2016). SPH-DEM model for free-surface flows containing solids applied to river ice jams. *Journal of Hydraulic Research* 54(1), 27–40.
- Sun, P. N. (2018). *Study on SPH Method for the Simulation of Object-Free Surface Interactions*. Ph. D. thesis, Harbin Engineering University, Harbin, China.
- Sun, X. S., M. Sakai and Y. Yamada (2013). Three-dimensional simulation of a solid-liquid flow by the DEM-SPH method. *Journal of Computational Physics* 248, 147–176.
- Tian, X. and D. C. Wan (2019). Simulation of sloshing in three-dimensional cylindrical tank by MPS method. *Chinese Journal of Ship Research* 14(3), 116–121.
- Wang, X. J., G. M. Zhang, W. T. Liu and Z. Zhou (2002). Computations of elastic-plastic waves by smoothed particle hydrodynamics. *Explosion and Shock Waves* 22(2), 97–103.
- Xu, Y., Q. C. Sun, L. Zhang and W. B. Huang (2003). Advances in discrete element methods for particulate materials. *Advances in Mechanics* 33(2), 251–260.
- Zhang, S. C. (1996). Smoothed particle hydrodynamics (SPH) method (A Review). *Chinese Journal of Computational Physics* 13(4), 385–397.
- Zheng, W. G., Y. Wang, Y. Y. Zhang, L. Q. Ren and S. L. Gu (2020). SPH method-based study on energy dissipation characteristics of stepped spillway. *Water Resources and Hydropower Engineering* 51(12), 117–124.